Cloud Properties Determined From GOES and MODIS Data During TC4

Patrick Minnis[1], Louis Nguyen[1], Rabindra Palikonda[2], J. Kirk, Ayers[2], Robert F. Arduini[2], Fu-Lung Chang[3], Thad L. Chee[2], David R. Doelling[1], Patrick W. Heck[4], Mandana M. Khaiyer[2], Michele L. Nordeen[2], William L. Smith, Jr.[1], Douglas A. Spangenberg[2], Christopher R. Yost[2], Ping Yang[5], Yu Xie[5]

[1]NASA Langley Research Center, Hampton, VA 23681
[2]Science Systems and Applications, Inc., Hampton, VA 23666
[3]National Institute of Aerospace, Hampton, VA 23666
[4]Cooperative Institute for Meteorological Satellite Studies, Madison, WI
[5]Department of Atmospheric Sciences, Texas A&M University, College Station, TX 77843

For *Journal of Geophysical Research* Special Issue on TC4

September 2009

Abstract

Satellite data taken during the 2007 Tropical Composition, Clouds and Climate Coupling Experiment (TC4) in Costa Rica provide the large-scale context for studying cloud, humidity, and radiation interactions in this tropical convective environment. Data from the Tenth and Twelfth Geostationary Operational Environmental Satellite (GOES-10/12) imagers and the MODerate-resolution Imaging Spectroradiometer (MODIS) on the Terra and Aqua satellites are analyzed with several different techniques to produce single and multilayered cloud properties and top-of-atmosphere radiative fluxes. The GOES-12 data are available nearly every half hour, while the MODIS data are available during the day around 1030 and 1330 LT. The cloud products and satellite imagery are available in various formats and accessible on the world wide web to facilitate comparisons with other observations and model results. The clouds over the TC4 domain (5°S – 25°N, 70°W – 100°W) vary dramatically over the diurnal cycle with maxima in clouds during the night over ocean and during the evening over land. The strongest convective activity occurs around the Isthmus of Panama with average ice water paths exceeding 700 gm^{-2} over some areas during the experiment period (17 July – 8 August 2007). Stratus clouds cover much of the Pacific part of the domain at an average altitude around 1.5 km. The average coverage at night is roughly 30% greater than that during the day. Clouds over the Gulf of Mexico and Caribbean Sea were infrequent and thin, except over islands and coastlines.

1. Introduction

The 2007 Tropical Composition, Clouds and Climate Coupling Experiment (TC4) in Costa Rica was designed to address a number of questions related to the interactions among convection, clouds, and humidity in the tropical upper troposphere (UT) and lower stratosphere [*Toon et al.*, 2009]. These questions include, among others, determining the physical mechanisms controlling changes in the UT humidity and the distribution of thin cirrus in the tropical tropopause layer (TTL) and its influence on radiative heating and vertical transport, quantifying the effects of convective intensity and aerosols on cirrus anvil properties, and characterizing the evolution and radiative impact of tropical anvils and cirrus over their life cycles, and validating satellite retrievals of various related parameters. The Tropics are governed by strong diurnal variations in convection and cloud cover driven by radiation, terrain, and dynamics. Thus, answering the TC4 questions and modeling the tropical large- and mesoscale processes necessarily requires some understanding of the diurnal cycle of the cloud systems.

Headquartered at Juan Santamaria Airport in San Jose, Costa Rica (10.0°N, 84.22°W), TC4 addressed its objectives by deploying 3 aircraft and several ground-based systems complemented by 7 different satellites. Most of the space-based measurements were taken from 5 low-Earth-orbiting satellites with advanced sensors that measure chemical, aerosol, and cloud-related parameters. While providing data critical for the experiment, these satellites take data only once during the daytime and once at night. Because of safety and logistical constraints, the aircraft missions were typically limited to the hours of 1230 – 2030 UTC (0730 – 1530 LT), missing the most intense late afternoon thunderstorms over the airport. Besides the surface radars, the only instruments capable of taking measurements over the full diurnal cycle in that area were the Tenth and Twelfth Geostationary Operational Environmental Satellites (GOES-10/12). In addition to covering the complete diurnal cycle, GOES provides the large-scale context for the flight missions and the experiment as a whole.

During TC4, GOES imagery was analyzed in near-real time providing the mission teams with images and estimates of cloud properties useful for planning and altering flights to maximize safety and success in meeting the flight objectives. After TC4 ended, the GOES data were re-analyzed using calibration and algorithm upgrades that became available after 2007. This paper provides an overview and summary of the cloud and radiation properties and products derived from the GOES data during the entire experiment and from MODerate-resolution Imaging Spectroradiometer (MODIS) data taken during the flight days using a common set of analysis algorithms.

2. Data

The greater TC4 domain, 5°S – 25°N and 70°W - 100°W, was selected to ensure that all of the envisioned flight missions would be encompassed. Although the experiment officially operated within the greater domain site between 17 July and 8 August 2007, science flights were conducted in transit to and from the United States before and after the experiment, thus expanding the science dataset from 13 July to 13 August 2007 [*Toon et al.*, 2009]. The primary geostationary satellite imagery used for this experiment was taken by GOES-12 situated on the Equator at 75°W. Imagery from GOES-10 at 60°W was also used to complement the GOES-12 at certain times when the GOES-12 scan was limited in its southward extent. The GOES-10 data were also analyzed in the same fashion as the GOES-12 data after the experiment, but only for the duration of the missions on flight days. Both the GOES-10 and 12 imagers have a nominal nadir spatial resolution of 4 km with four channels in common: visible (VIS, 0.65 µm), shortwave infrared (SIR, 3.9 µm), water vapor (WV, 6.7 µm), and infrared (IR, 10.8 µm). The fifth channels on GOES-10 and 12, respectively, are the split window (SPW, 12.0 µm) and CO2-slicing (COS, 13.3 µm, 8-km resolution). The VIS data were taken at a 1-km resolution and averaged up to 4 km. The 1-km images were mostly used for mission support.

The VIS channels were calibrated against the Terra MODIS Collection-5 channel-1 (0.64 µm) radiances every 3rd month from May 2003 through February 2008 following the method of *Minnis et al.* [2002]. The VIS reflectance is

$$R = L_v / S_o / \mu_o / ESD, \quad (1)$$

where the reference solar constant, S_o = 526.9 Wm^{-2} sr^{-1} µm^{-1}, μ_o is the cosine of the solar zenith angle SZA, *ESD* is the Earth-sun distance correction factor, and the radiance,

$$L_v = (a_0 + a_1\, d + a_2\, d^2)\,(C - C_o), \quad (2)$$

is given in Wm^{-2} sr^{-1} µm^{-1}. C is the observed brightness count, the space count, C_o = 29, and the number of days since the reference date is represented by d. For GOES-10 and 12, the reference dates are 27 April 1998 and 1 April 2003, respectively. Values for the coefficients, a_0, a_1, and a_2, are, respectively, 0.5319, 1.894 x 10^{-4}, and -2.11 x10^{-9}, for GOES-10 and 0.6198, 8.81 x 10^{-5}, and 0.0 for GOES-12. The GOES-10 coefficients are only valid for dates after 1 January 2000. The nominal GOES calibrations are used for all of the other channels.

MODIS data from Terra and Aqua were taken and analyzed only for the flight days during the times of the overpasses. MODIS is a 36-channel imager with a common nominal resolution of 1 km although resolutions of 0.25 or 0.50 km are available for a small subset of channels [*Barnes et al.*, 1998]. Channels 1 (VIS, 0.645 µm), 6 (NIR, 1.61 µm), 20 (SIR, 3.8 µm), 31 (IR, 11.03 µm), and 32 (SPW, 12.02 µm) are used here at the 1-km resolution. For a given scene, the Aqua VIS channel reflectances are 1% greater than their Terra counterparts [*Minnis et al.*, 2008a]. The Aqua channel-6 brightness temperatures are, on average, 0.55 K than their Terra counterparts during daytime [*Minnis et al.*, 2008b]. The IR and SPW channels on Aqua appear to be accurate to better than 0.1 K [*Tobin et al.*, 2007].

Temperature and humidity profiles from numerical weather prediction (NWP) models were used to compute expected spectral clear-sky temperatures and to account for the atmospheric attenuation of the spectral radiances during the experiment. The near-real time retrievals used the NOAA 6-hourly 1.25° Global Forecast System analyses [*Kalnay et al.*, 1990]. The post-experiment analyses employed the Meteorology, Ozone, and Aerosol (MOA) product from the Clouds and the Earth's Radiant Energy System (CERES) project [*Gupta et al.*, 1997], which combines ozone profiles from the product of *Yang et al.* [2006] and temperature and humidity profiles from Version 5 of the Global Modeling Assimilation Office GEOS-5 numerical weather analyses [*Bloom et al.*, 2005]. The GEOS-5 profiles and skin temperatures were available on a 1° grid every 6 and 3 hours, respectively. The MOA product performs interpolations to provide hourly temperature and humidity data at the 0.5° resolution used for processing and averaging. All other ancillary input data are the same as those employed by *Minnis et al.* [2008b].

3. Methodology

Cloud and radiation parameters were derived from the satellite data at the pixel scale. In addition to averaging the data, a variety of products were computed that matched the imagery and retrieved parameters with the TC4 flight data. All of these products are available on the World Wide Web at http://www-angler.larc.nasa.gov/tc4/. The data were analyzed in near-real time with one set of algorithms and 2 years later using a revised set of algorithms. While the latter are the main focus of this paper, both sets are discussed because some of the near-real time products have been employed in other studies. The newer products are more accurate than the near-real time products. Table 1 lists the parameters available at the pixel level for the post-experiment results. The variables BTD, VZA, and RAA refer to brightness temperature difference, viewing zenith angle, and relative azimuth angle, respectively. All other variables are explained below.

3.1 Daytime satellite retrievals

The cloud properties were derived from the GOES and MODIS data using variants of the CERES Edition-2 cloud analysis algorithms. Each pixel is first classified as being clear or cloudy using a version of the methodology of *Minnis et al.* [2008b] that is appropriate for the complement of channels on the particular imager. *Minnis et al.* [2009] describe the retrieval methods in detail. They are briefly reviewed here and variants are noted when applicable.

During daytime (SZA > 82°), the cloudy pixels were analyzed with the Visible-Infrared-Shortwave-infrared-Split-window Technique (VISST) that retrieves cloud effective temperature T_c, phase, optical depth τ, and effective droplet radius r_e or ice crystal diameter D_e, depending on the phase. The phase is determined using a sequence of tests. A few of the tests use the SPW channel. Because the SPW data are not available, those specific tests are not used in the VISST for GOES-12. The ice crystal effective diameter can be converted to an equivalent effective droplet radius with the following formula:

$$r_e = (7.918 \times 10^{-9} D_e^2 + 1.0013 D_e + 0.4441) D_e \quad (3)$$

The reflectance models of *Minnis et al.* [1998], based on various droplet size distributions and smooth hexagonal column ice crystal size distributions, were used in the near-real-time retrievals. The post experiment retrievals used the same water droplet models, but replaced the smooth hexagonal column reflectances with those computed using rough hexagonal columns having the same size and shape as the smooth crystal distributions. The latter were computed for the VIS and SIR channels with a roughness factor of 1.0 using the methods of *Yang et al.* [2008a, b]. The roughened crystals yield smoother phase functions with slightly smaller asymmetry factors than their smooth counterparts. Ice or liquid water path, IWP and LWP respectively, is computed from the particle size and optical depth for each pixel.

Cloud effective height Z_c and pressure p_c, which nominally correspond to the equivalent radiating center of the cloud, are estimated from T_c using a lapse-rate adjusted temperature profile. For pressures, p > 700 hPa, the temperature profile is

$$T(z + z_o) = T_o + \Gamma (z - z_o) \quad (4)$$

where z_o is the surface elevation above mean sea level and Γ is the lapse rate and is set to -7.1K km^{-1} for the near-real time analyses. The post-experiment processing used Γ = -7.7 K km^{-1} and -6.5 K km^{-1}, respectively, over ocean and land. Over ocean and land surfaces, the value of T_o is, respectively, the sea surface temperature or the surface air temperature from the NWP analyses. Between 700 and 500 hPa, Γ is adjusted to ensure that the resulting temperature at 500 hPa equals that in the NWA profile. For $p \leq 500$ hPa, the NWP vertical profile of atmospheric temperature remains unchanged. If $T_o < T_c$, then Z_c is set, as a default, to 0.5 km above the surface elevation. The pressure corresponding to Z_c is assigned to p_c. The physical tops Z_t and bases Z_b of the clouds are estimated using a set of empirical formulae described by *Minnis et al.* [2009]. For optically thick ice clouds, it is assumed that the cloud-top temperature $T_t = T_c$ and, therefore, $Z_t = Z_c$. Because earlier field programs revealed that Z_t is often underestimated by 1-2 km when using that assumption for optically thick ice clouds [*Sherwood et al.*, 2004], the empirical formula from *Minnis et al.* [2008c] is used for the post-experiment retrievals for ice clouds having $\tau > 10$.

Several other algorithmic changes were made for post-experiment processing. The ozone transmittance used to account for VIS absorption by the atmosphere in the near-real time (CERES Ed2) processing is

$$t_{O3} = \exp\text{-}\{u\,(0.085 - 0.00052\,u)\,(1/\mu_o + 1/\mu)\}, \qquad (5)$$

where u is computed in cm STP for the layer between the TOA and 300 hPa, and μ is cosine of viewing zenith angle VZA. This formula is based on the filter function for an older generation of GOES imagers and tends to overestimate t_{O3} for the VIS channels on most new imagers causing an overestimate of τ. For MODIS and GOES, t_{O3} is multiplied by 0.86 and 0.88, respectively. These correction factors are based on radiative transfer calculations using the actual spectral filter functions for each imager. Because the GFS profiles do not include ozone, a constant value of 320 Dobson units was used to compute u. in the near-real time retrievals. This value is more typical for the midlatitudes. A value of ~280 Dobson units is more appropriate for tropical regions. Thus, t_{O3} was overestimated even more for the near-real time processing than due just to the use of (5).

For the real-time processing, the Rayleigh scattering optical depth of $\tau_R = 0.0486$ for one atmosphere was used for both MODIS and GOES. Because of the differences in the spectral response functions, that value underestimates the Rayleigh contribution to the GOES-observed reflectance. In the GOES post-experiment processing, $\tau_R = 0.0562$. This more accurate value of τ_R in the post-processing results in a small decrease in the retrieved cloud optical depth.

An addition to the post-experiment processing retrievals involves the use of the COS channel for post-experiment retrievals. The COS was used together with the IR channel to retrieve the emissivity, temperature, height, and pressure, ε_M, T_M, Z_M, and p_M, respectively, for high clouds using the modified CO_2-absorption technique (MCO2AT) of *Chang et al.* [2009a,b]. The MCO2AT retrieves both T_t and the background temperature T_{bg}. The latter corresponds to either the clear-sky temperature or the temperature T_L of a lower cloud. The MCO2AT results are used to produce a separate output dataset for pixels identified as containing multi-layered (ML) clouds. The VISST assumes that the clouds in a given pixel are single-layered (SL). Thus, if a thin cirrus overlaps a low water cloud, the VISST will obtain values of T_c and p_c that correspond to a height somewhere between the lower and upper cloud and the water in the column will be considered as all ice or water depending on how the radiances are interpreted. Clouds are identified as being ML in a manner similar to that used by *Chang and Li* [2005]. The MCO2AT emissivity, ε_M, is converted to an equivalent VIS optical depth τ_M and compared to the VISST-retrieved τ. If the two optical depths differ significantly and $\tau > 3.6$, then the pixel is classified as ML ($\varepsilon_M < 0.75$), likely ML ($0.75 \leq \varepsilon_M < 0.95$), or weak ML (often multi-phased SL) cloud depending on the ε_M, τ, and τ_M. The last category corresponds to optically thick clouds with $\varepsilon_M >$

0.95, $\tau > 22.5$, and, $T_c < 223$ K. The upper and lower cloud temperatures are $T_U = T_M$ and $T_L = T_{bg}$, respectively. However, certain adjustments of T_L are made by averaging T_L with the nearby single-layered low-cloud pixel T_c if $T_c > T_L$. This is because T_{bg} could be underestimated if the upper layer is geometrically thick but optically thin. The corresponding heights and pressures are determined from those temperatures. The upper-layer cloud optical depth τ_U is equal to τ_M and the lower-layer cloud optical depth τ_L is computed as in *Minnis et al.* [2007] using the ML cloud reflectance models. The lower cloud droplet effective radius r_L is currently assumed as being the averaged r_e from nearby water-cloud pixels. The upper cloud effective ice diameter D_U is retrieved as in VISST, except the background radiance is computed as a function of the corresponding τ_L, T_L and r_L values and the surface properties..

Broadband shortwave (0.2 – 5 µm) albedo α_{SW} and outgoing longwave (5 – 100 µm) radiation (OLR) fluxes M_{LW} were estimated from the GOES-12 VIS and IR radiances, respectively, using empirical formulae. Those functions are based on matched GOES-8 narrowband data and Terra and Aqua CERES ERBE-like broadband measurements taken over the southern Florida area (22°N – 31°N, 75°W – 88°W) during July 2002. The data were matched, correlated, and used in regression analyses to determine coefficients for the formulae over ocean and land separately following the methods of *Minnis and Smith* [1998]. The shortwave albedo is estimated as

$$\alpha_{SW} = a_0 + a_1\, \alpha_{VIS} + a_2\, \alpha_{VIS}^2 + a_3 \ln(1/\mu_o), \qquad (6)$$

where α_{VIS} is the VIS albedo as determined as in *Minnis and Smith* [1998]. Because there was little variation in the SZA for the matched data, a constant value of 0.07 is used for a_3 to minimize any overestimate of α_{SW} at large SZAs.

The OLR is computed as follows.

$$M_{LW} = a_0 + a_1 M_{IR} + a_2 M_{IR}^2 + a_3 \ln(\mathrm{CRH}), \tag{7}$$

where M_{IR} is the IR flux and CRH is the column relative humidity above the cloud level. They are computed as in *Minnis and Smith* [1998]. Table 2 lists the coefficients determined for Eqs (6) and (7) using separate fits over land and ocean for α_{SW} and a single fit for OLR. The squared correlation coefficients R^2 and standard errors of the estimate SE are also listed. All of the data are well correlated and the standard errors in α_{SW} for ocean and land are, respectively, 10 and 6% of the mean values.

3.2 Nighttime satellite retrievals

At night, defined as those hours when SZA > 82°, cloud properties were derived from the GOES and MODIS data using variants of Shortwave-infrared-Infrared-Split-window Technique (SIST) than normally employs only the SIR, IR, and SPW channels [*Minnis et al.*, 2009]. The real-time processing used the COS channel as if it were the SPW channel. Values of Z_c, T_c, and ε were also determined using the standard CO_2-absorption technique SCO2AT [*Chang et al.*, 2009a], which uses the surface temperature from the sounding to compute the background temperature. The SCO2AT values replaced the SIST results whenever ε(SCO2AT) < 0.98. In the most recent processing, the MCO2AT was used to determine cloud emissivity and, therefore, height and temperature. Particle sizes were estimated by matching the 3.9-11 μm brightness temperature differences to model values in the same manner used by the SIST. The nighttime results are mostly usable for cloud amount and height. The cloud microphysical properties are not very accurate and, while included in the output, should not be used.

3.3 Data averaging

In addition to providing the pixel results, averages were computed for each parameter in a given 0.5° region at each image time for GOES-12 for water and ice clouds separately. Averages were also computed for low, middle, and high clouds defined as having $Z_c < 2$ km, 2 km $< Z_c \leq 6$ km, and $Z_c > 6$ km, respectively. These regional averages were used to compute the mean values for over 70 parameters for the entire period at each time slot .

3.4 Data matching

To facilitate comparisons with the aircraft (DC-8, ER-2, and WB-57) data and provide contextual images for the flights, the flight tracks were plotted on the radiance images and the product files. Additionally, averages of the parameters for the pixels corresponding to the flight tracks were computed for each aircraft using the GOES-10/12, Terra, and Aqua data. After parallax correction using Z_c, the mean values of a given parameter were computed using the four pixels nearest the aircraft latitude and longitude roughly every 5.4 s for the image taken closest in time to the aircraft measurement. The aircraft flight tracks were obtained in near-real time from the output of the aircraft navigation systems. For the post experiment processing, the navigation files were obtained from the Earth Science Project Archive web page (http://espoarchive.nasa.gov/archive/arcs/tc4/data). GOES-12 results were also matched to the Cloud-Aerosol Lidar In Space Observations (CALIPSO, [*Winker et al.*, 2007]) satellite ground track.

4. Products

The data products discussed in this section are accessible at the world wide web url, http://www-angler.larc.nasa.gov/tc4/. Other products that are not discussed, but are also available at that website, include a satellite orbit and viewing predictor tool and KML files for Google Earth plotting. Because of space limitations, only a few examples and summaries of a few parameters are presented here.

4.1 Flight track imagery and products

Figure 1 shows the DC-8 and ER-2 flight tracks plotted on GOES visible channel imagery taken during the 24 July 2007 mission. Individual segments corresponding to ~30 min centered on the image times are plotted in Figures 1a-1c. The insets in the lower right show plots of the aircraft altitude in km above MSL. To cover the entire domain, GOES-10 and GOES-12 images were stitched together because the GOES-12 only covers areas north of the Equator, except at the 8 synoptic hours (0, 3, 6,…21 UTC), and the GOES-10 only covers areas south of ~10°N. The ER-2 (blue) flew at 20 km while the DC-8 (red) altitude ranged from near the surface to 12 km during the mission. Around 1345 UTC (Figure 1a), the DC-8 crossed under the ER-2, sampling clouds below 6 km. An hour later (Figure 1b), it flew a loop under the ER-2 while rising up to ~12 km. At 1545 UTC (Figure 1c), the DC-8 dropped 1 – 2 km lower in a spiral before returning to base. The ER-2 continued taking remote measurements until 1845 UTC. Complete flight tracks for the day's mission are plotted on the 1528 UTC image in Figure 1d.

Similar images are available for each image time during the mission and for the IR channel and 5 retrieved parameters, T_c, Z_c, IWP, τ, and D_e. On the cloud property images, the satellite-estimated cloud base and top heights are plotted in the inset graphs. Both loops and individual images are available. *Toon et al.* [2009] show summary images for each flight day.

Values for 22 different variables from each satellite can be extracted and plotted for every flight. Figure 2 shows plots of τ, D_e, IWP, and Z_t derived in real time from GOES-12 data for the 24 July 2007 flights shown in Figure 1. Standard deviations, though available, are not shown. These plots provide a quick overview of the clouds sampled during each flight and can be tailored to the time segment of interest. During the first 3 hours of the mission, the ER-2 (Figure 2a) sampled many optically thick clouds with IWP values reaching 4500 gm^{-2} and particle sizes varying from ~15 to 130 μm. The greatest value of Z_t for the flight was 15.5 km. Although the DC-8 (Figure 2b) flew underneath the ER-2 at times during the mission, it often sampled different clouds. The maximum value of IWP for the DC-8 flight is 4300 gm^{-2} at ~1500 UTC. In addition to the plots, ascii files containing all of the matched data or selected times and parameters can downloaded.

4.2 Satellite imagery and cloud products

Both single and multiple channel and brightness temperature difference images and pixel-level data are available along with all of the parameters listed in Table 1. Figure 3 shows pseudocolor images for data taken around 1540 UTC, 24 July 2007. These images were created by assigning red, green, and blue (RGB) to the VIS, IR, and SIR channels, respectively, and normalizing the intensities to the observed range in each parameter. These RGB images are useful for quickly discriminating between high and low clouds and between bright and dark clouds, and for identifying potentially overlapped clouds. The Terra MODIS image (Figure 3b) was taken ~10 min before the combined GOES-10/12 image and reveals much greater detail in the clouds albeit over a smaller area. The sunglint area in the GOES-12 image east of Nicaragua and north of Columbia and Venezuela is reduced in size by using the full extent of the GOES-10 data in Figure 3a.

The retrievals of D_e for these images are shown in Figure 4. The real-time (RT) values are shown for GOES-10 (Figure 4a), 12 (Figure 4b), and Terra MODIS (Figure 4d), while the revised VISST with the rough ice crystal model results are shown for GOES-12 (Figure 4c). In general, all of the retrievals yield similar patterns. However, the GOES-10 values tend to be larger than those from GOES-12 RT eastward of Costa Rica and smaller to the west. The Terra values appear to be very similar to those from GOES-12 RT with the largest crystals occurring near the cores of the convective cells, as reported by Bedka and Minnis [2009]. The rough-crystal values of D_e are typically smaller than from any of the RT results. This decrease in D_e is most likely the result of using the rough crystal model. Results like those in Figure 4 are available for all of the parameters. Given that the revised VISST should be the most accurate of the retrievals, only the post-processing results from GOES-12 are discussed hereafter unless otherwise noted.

5. Results

Because of the wide variety of results that could be presented, only a sampling is shown here. The reader is encouraged to examine the results in detail at the noted World Wide Web address.

5.1 Revised VISST retrievals

The distributions of average cloud cover for the entire experiment are plotted in Figures 5 and 6. Total cloud cover (Figure 5a) is greatest west of 75°W over the Pacific and Central America. South of 5°N, much of that cloudiness consists of low-level liquid clouds (Figure 5b). Elsewhere, the liquid cloud cover varies from 15 -35%. The diurnal variation of mean TC4 ice cloud cover is shown as 3-hourly averages in Figures 6a-h along with the average for all hours (Figure 6i). At 0115 UTC (1815 LT), the maximum ice cloud cover occurs over the land areas in western Central America and around the Gulf of Venezuela with a broad area extending southwestward from the Costa Rica-Panama border area. Those maxima fade over the ensuing 6 hours so that by 0200 LT (Figure 6c), a broad maximum appears over northern Columbia. By 1015 UTC (Figure 6d), the maximum has moved westward and split with a new maximum forming over the Panama Bight. During the morning after sunrise (Figures 6e, f), the maxima are found only over water, mainly along the Panamanian and Columbian coasts By 1915 UTC, the peak ice cloud coverage has shifted westward remaining mostly over water, although maxima appear over parts of the Isthmus of Panama and eastern Nicaragua. A broad area of high cloudiness south of Mexico around 13°N, 98°W reaches its greatest extent at this time also. By late afternoon at 2215 UTC (Figure 6h), most of the high cloud cover is back over land. The maximum near the Pacific coast of Costa Rica has moved offshore to the southwest. On average, most high cloudiness occurs over water south of the Isthmus and Mexico (Figure 6i) separated by a relative minimum near 10°N, 90°W.

The distributions of mean cloud top heights are plotted in Figure 7. In the southwest part of the domain, where liquid water clouds dominate, the average heights are between 0.8 and 2.0 km (Figure 7a), while over the areas where ice clouds reign, the mean heights rise up to 10 km. The liquid water clouds over much of the open ocean are below 2 km, on average (Figure 7b), while the mean liquid water cloud heights are as high as 6 km over some land areas. The mean ice cloud top heights are generally over 10 km in the main areas of convective activity, dropping off to less than 7 km in the western part of the domain.

Figure 8 shows the vertical distribution of cloud heights for day and night over the land and ocean areas separately. A pronounced low-cloud peak is obvious over ocean during both day and night (Figures 8a, c) with the maximum in low clouds occurring during the night at an altitude of

~ 1.3 km. This diurnal change is typical for the marine stratus west of South America. The vertical profiles over ocean show a more pronounced minimum at 5 km and well-defined maxima 12, 13.5, and 16 km during the night. The peaks are nearly the magnitude and contrast with the minimum by ~1.5%. During the daytime, the 13.5-km maximum disappears and the 16-km frequency drops by about one third. The 12-km peak is the same magnitude as that during the night, but its contrast with the 5-km minimum decreases by a third. Over land, the low clouds are most frequent around 2.5 km during both day and night (Figures 8b, d). The minimum is found between 7 and 7.5 km. The cloud-top frequencies above 8 km follow a pattern similar to that seen over water. The 12, 13.5, and 16-km maxima are prominent at night, but the 13.5-km peak fades during the daytime. The contrast between the maxima and the 7-km minimum is also more notable at night. However, the high clouds account for a larger percentage of the clouds over land compared to ocean, so the frequency maxima are greater than their ocean counterparts. A relative maximum is seen during the day over land. Presumably, this occurs mostly over mountainous terrain along the Andes and western parts of Central America (e.g., Figure 7b).

The differences in the high cloud maxima between day and night mostly reflect the diurnal cycle of convection. As pointed out by *Bedka and Minnis* [2009], the extremes in convective cloud cover over both land and ocean occur around terminator or during the night. However, the exact shapes of the profiles may be influenced by the change in algorithms from day to night. The latter uses the MCO2AT, which is less influenced by underlying clouds than the VISST used during the daytime. [*Chang et al.*, 2009b] Thus, some high clouds occurring above low clouds are more likely to be placed in the middle levels during the daytime than at night. This tendency was also found for the SIST when applied to data over Oklahoma [*Xi et al.*, 2009]. Thus, the diminished contrast between the convective cloud peaks and the midlevel minima over land and ocean during the day is likely due to the impact of multilayered clouds, which are discussed section 5.2. *Bedka and Minnis* [2009] provide a detailed analysis of the convective cloud diurnal cycles during TC4 using the dataset described here.

During daytime, the cloud optical depths (Figure 9) are greatest from the northern border of Costa Rica southward over the Pacific down to ~3°S and eastward to the coast. The maximum mean τ for water clouds occurs west of Ecuador and over the Andes (Figure 9a), while the minima are over the southern Caribbean and Gulf of Mexico. The few ice clouds that occur over the southwestern part of the domain are very thin with $\tau < 1$ in most cases (Figure 9b). The thickest ice clouds are concentrated around the Panama and Costa Rica. A secondary maximum near 9°N, 97°W is apparent over the open Pacific. Except for land in the Caribbean, the ice cloud optical depths are generally quite small.

In general, the mean water droplet and ice crystal sizes over land significantly smaller than those over water (Figure 10). The largest mean values of r_e, ~20 µm (Figure 10a), occur over the Gulf of Mexico. These and other large values in the Gulf are associated with small cloud fractions (Figure 5b) and optical depths (Figure 9a). Other relatively large values of r_e over the Pacific are associated with larger values of τ and cloud fraction. In general, the values of re over water are ~2 µm larger than those found from MODIS on Terra and Aqua. Over land, the differences are typically less than 1 µm. This difference may be due to the larger pixel sizes and the greater range of SZA covered by the GOES-12 measurements. The values of D_e over land are mostly around 40 µm (Figure 10b) compared to ~55 µm over water. The largest mean values ~ 65 µm around found in the areas with the most ice clouds, near the Isthmus.

Because of the small optical depths, the water clouds over the Atlantic side of Central America have very small mean LWPs, < 50 gm^{-2}, compared to those over the Pacific that peak around 175 gm^{-2} off the Ecuadorian coast. The mean IWP mostly follows the patterns in τ, since the average D_e is not particularly variable from region to region. The maximum values approach 1000 gm^{-2} in the Bight of Panama. Table 3 provides a summary of the mean parameter values for the entire domain. The cloud fractions and heights are given for all 24 hours, while the remaining parameter values are only for daytime.

The ice water path follows a cycle similar to that in Figure 6, as seen in Figure 12, which shows only the daytime IWP averages every 3 hours. At 1315 UTC, the mean IWP reaches a maximum exceeding 1000 gm^{-2} over areas in the Panama Bight. Relative maxima occur 10° south of the Mexican coast and just off the Guatemala Pacific coast. A minimum in IWP over the domain occurs around 1545 UTC, just half an hour before the values shown in Figure 7b, which has smallest values over all for the images shown. The depth of the clouds slowly increases throughout the remainder of the morning before a faster buildup during the afternoon (Figures 7c, d), particularly over land. Mean values of IWP again exceed 1000 gm^{-2} for a few areas over the Isthmus after 2100 UTC.

5.2 Multilayered cloud retrievals

Figure 13 shows an example of the single and multilayered cloud retrievals for GOES-12 data taken at 2015 UTC, 5 August 2007. The RGB image (Figure 13a) shows extensive areas of cirrus clouds extending over lower stratus in Pacific and over mostly clear air over the Caribbean Sea and Gulf of Mexico. The VISST (Figure 13b) classifies much of the cloud cover as ice phase (red) with most liquid water clouds (blues) occurring over the Pacific. Roughly half of VISST ice clouds are classified as being multilayered clouds of one sort or another, while some of the VISST liquid clouds are reclassified as multilayered (ML) clouds (Figure 13c). Clouds that are definitely ML, according to the classifier, are denoted by the magenta pixels. These pixels mostly occur in outer portions of anvils or as lone cirrus clouds over lower clouds. Other likely ML pixels are shown in yellow in Figure 13c. These typically occur closer to the convective core, which is often characterized as being weak ML (brown pixels). This classification finds that the background brightness temperature is greater than 233 K, but the ice cloud emissivity is quite high suggesting that there is a liquid water cloud below the thicker ice clouds. This most often is true for convective cores, but the cloud would not be multilayered in the classical sense since there are probably no gaps between the ice and water clouds. Thus, it is more a classification of a cloud having both phases, either mixed or in separate layers.

The second row of Figure 13 shows the cloud top heights. Except for the thickest clouds, the VISST cloud top heights Z_{top} (Figure 13e) are generally below the MCO2AT upper cloud heights Z_{UL} (Figure 13f) and higher than the lower cloud heights Z_L from the multilayer retrieval (Figure 13d). In most cases, Z_L is around the same level as the VISST low cloud heights when no upper cloud is present. In comparisons with the ER-2 Cloud Physics Lidar (CPL) measurements during TC4, *Chang et al.* [2009b] found that the MCO2AT-inferred mean Z_U values are slightly underestimated (~1 km) for SL clouds having ε_M between 0.5 and 0.9. For more opaque ($\varepsilon_M >$ 0.9) or more transmissive ($\varepsilon_M < 0.5$) clouds, the MCO2AT mean Z_U appears to have more underestimation as compared to the CPL data. However, the revised VISST cloud heights are nearly unbiased for clouds having emissivities greater than 0.9 as shown in Figure 13e for the convective cores when $Z_{top} > 14$ km. At lower emissivities, the revised VISST underestimates Z_{top} more than Z_U, especially for ML clouds.

Cloud optical depths are shown in the third row of Figure 13. The results seem to be quite reasonable for the definite and likely ML cases (Figure 13c) because τ_L is similar in magnitude to τ for nearby SL clouds in Figure 13h. Likewise, the values of τ_U are similar to those for SL ice clouds nearby. Most of the convective cores have values of $\tau > 100$ for the VISST results in Figure 13h. Values of $\tau_L > 100$, however, cover much more area in Figure 13g, while the values of τ_U do not exceed 8 for the convective cores (Figure xi). The increased number of optically thick pixels in Figure 13g is due to the partitioning of the ice and water in the weak ML cases. It is assumed in the retrieval that $\varepsilon = 0.98$, so no values of τ_U can exceed 8. For a given reflectance, the optical depth for a water droplet cloud is typically 1.5 times that for an ice cloud [*Minnis et al.*, 1993]. Thus, to match the convective core reflectance, τ_L must be considerably larger than τ from VISST, which interprets the reflectance as coming from a single cloud volume entirely composed of ice crystals. This partitioning of ice and water clouds in weak ML cases is unrealistic, so the values of τ_L and τ_U are not recommended for user applications until a more representative partitioning of the ice water in these deep convective clouds can be developed.

For the TC4 experiment as a whole, the ML detection algorithm classified 16.8% of all pixels as multilayered during daytime (SZA < 82°) and 6.6% of the pixels as ML during nighttime. Those values correspond to 26.8 and 9.1%, respectively, of the cloudy pixels. At night, significantly fewer pixels are classified as ML because of diminished optical depth information. The daytime value is probably more representative as a whole. While approximately a quarter of the clouds in this domain are actually high-over-low cloud systems, the percentage of ML pixels detected in Figure 13 is likely an underestimate since many of the very thin cirrus clouds are missed by both the VISST and MCO2AT [*Chang et al.*, 2009b]. Detection of those thin clouds with passive sensors remains a challenge.

6. Summary and Conclusions

Data sets consisting of cloud and radiative properties have been derived from various satellite imager radiances for a domain and time period encompassing all of the TC4 tropical flights. Preliminary estimates of the parameters have been replaced by new values based on new and revised algorithms. The VISST, the retrieval algorithm used during daytime, was modified to retrieve ice cloud properties using the scattering properties of roughened hexagonal ice columns instead of the smooth columns employed earlier. Ozone absorption and Rayleigh scattering in the retrieval parameterization were also corrected to better account for the GOES visible-channel spectral filter function. A new empirical method was used to estimate the physical cloud-top height of optically thick ice clouds from the effective radiating height. As a result of these changes, the revised VISST yields slightly lower optical depths and higher cloud-top heights. At night, the MCO2AT is used to determine the ice cloud-top temperature, which facilitates the retrieval of cloud optical depth and effective particle for semitransparent clouds. The MCO2AT and VISST were also used together to detect multi-layered clouds and to retrieve the properties of the clouds in each of the two cloud layers.

Both the MCO2AT and revised VISST yield more accurate cloud-top heights for ice clouds compared to the SCAO2AT and the original VISST, respectively [*Chang et al.*, 2009b]. The revised VISST produces ice cloud microphysical properties that are in good agreement with properties from in situ TC4 measurements [*Yost et al.*, 2009]. Thus, the results should be valuable for confidently studying the daytime variations of the ice cloud properties over the domain for the TC4 experiment. At night, the microphysical properties are less reliable and should probably not be used. However, the nighttime ice cloud-top heights are as accurate, if not more accurate than the daytime values. This, the retrieved cloud heights and amounts should be reasonable for all times of day. The daytime liquid cloud properties are similar to those obtained using VISST with other imagers and validated against independent reference datasets. The multilayered cloud properties also appear to be quite reasonable except for the weak multilayer cases. Those thick ice-over-water systems, which are mostly convective cores for TC4, require more study to determine the best way for partitioning ice and water within the cloud. The properties of multilayered clouds at night also need further examination.

The clouds within the TC4 domain follow a very complex diurnal cycle that is primarily characterized by late afternoon deep convection that peaks around sunset over most land areas and nocturnal maxima in the deepest convection over water. This simplification masks a more complex geographically diurnal sequence that appears to be driven by interactions of land and sea breezes with the highly variable terrain. As reported by *Bedka and Minnis* [2009], the diurnal variations in convection appeared to be similar to the available climatology for the region. Thus, the TC4 measurements should be fairly typical of the clouds in the area, at least for daytime. Any conclusions about the interactions of convection and moisture in the tropical tropopause in this region must take the extreme diurnal changes into account. It is hoped that the dataset reported here will be valuable for that purpose and for other studies of the highly variable cloud systems in this part of the world.

Acknowledgments

This research was supported by the NASA Radiation Science Program TC4 project, the NASA Applied Sciences Program, and the Department of Energy Atmospheric Radiation Measurement Program through Interagency Agreement, DE-AI02-07ER64546. Thanks to Marilyn Vasques for providing the DC-8 navigation data in real time.

References

Barnes, W. L., T. S. Pagano, and V. V. Salomonson (1998), Prelaunch characteristics of the Moderate Resolution Imaging Spectroradiometer (MODIS) on EOS–AM1, *IEEE Trans. Geosci. RemoteSens., 36*, 1088–1100.

Bedka, K. M. and P. Minnis (2009), GOES-12 observations of convective storm variability and evolution during the TC4 field program, Submitted to *J. Geophys. Res.*

Bloom, S., and Co-authors (2005), Documentation and validation of the Goddard Earth Observing System (GEOS) data assimilation system—Version 4, NASA Goddard Space Flight Center, Greenbelt, MD, *Tech. Rep. Series on Global Modeling and Data Assimilation 104606*, 165 pp.

Chang, F.-L., and Z. Li (2005), A new method for detection of cirrus overlapping water clouds and determination of their optical properties, *J. Atmos. Sci.*, *62*, 3993–4009.

Chang, F.-L., P. Minnis, J. K. Ayers, M. J. McGill, R. Palikonda, D. A. Spangenburg, William L. Smith, Jr., and C. R. Yost (2009b), Evaluation of a satellite-based upper-troposphere cloud height retrievals in multi-layer cloud conditions during TC4, Submitted to *J. Geophys. Res.*

Chang, F.-L., P. Minnis, B. Lin, M. Khaiyer, R. Palikonda, and D. Spangenberg (2009a), A modified method for inferring upper-troposphere cloud-top height using the GOES-12 imager 10.7- and 13.3-µm data, *J. Geophys. Res.*, in revision.

Gupta S. K., A. C. Wilber, N. A. Ritchey, F. G. Rose, T. L. Alberta, T. P. Charlock, and L. H. Coleman (1997), Regrid humidity and temperature fields (system 12.0). CERES Algorithm Theoretical Basis Document Release 2.2, *NASA/RP-1376*, 20 pp. [Available online at http://asd-www.larc.nasa.gov/ATBD/ATBD.html.]

Kalnay, M. Kanamitsu, and W.E. Baker (1990), Global numerical weather prediction at the National Meteorological Center, *Bull. Amer. Meteor. Soc.*, *71*, 1410-1428.

Min, Q, P. Minnis, and M. M. Khaiyer (2004), Comparison of cirrus optical depths from GOES-8 and surface measurements. *J. Geophys. Res.*, *109*, D20119, 10.1029/2003JD004390.

Minnis, P., D. R. Doelling, L. Nguyen, W. F. Miller, and V. Chakrapani (2008), Assessment of the visible channel calibrations of the TRMM VIRS and MODIS on *Aqua* and *Terra*, *J. Atmos. Oceanic Technol.*, *25*, 385-400.

Minnis, P., D. P. Garber, D. F. Young, R. F. Arduini, and Y. Takano (1998), Parameterization of reflectance and effective emittance for satellite remote sensing of cloud properties, *J. Atmos. Sci.*, *55*, 3313-3339.

Minnis, P., P. W. Heck, and D. F. Young (1993), Inference of cirrus cloud properties using satellite-observed visible and infrared radiances, Part II: Verification of theoretical cirrus radiative properties, *J. Atmos. Sci.*, *50*, 1305-1322.

Minnis, P., L. Nguyen, D. R. Doelling, D. F. Young, W. F. Miller, and D. P. Kratz (2002), Rapid calibration of operational and research meteorological satellite imagers, Part I: Evaluation of research satellite visible channels as references, *J. Atmos. Oceanic Technol.*, *19*, 1233-1249.

Minnis, P. and W. L. Smith, Jr. (1998), Cloud and radiative fields derived from GOES-8 during SUCCESS and the ARM-UAV Spring 1996 Flight Series, *Geophys. Res. Lett.*, *25*, 1113-1116.

Minnis, P., S. Sun-Mack, and Co-authors (2009), Cloud property retrievals for CERES using TRMM VIRS and Terra and Aqua MODIS data. *IEEE Trans. Geosci. Remote Sens.*, submitted.

Minnis, P., Q. Z. Trepte, and Co-authors (2008b), Cloud detection in non-polar regions for CERES using TRMM VIRS and Terra and Aqua MODIS data, *IEEE Trans. Geosci. Remote Sens.*, *46*, 3857-3884.

Minnis, P., C. R. Yost, S. Sun-Mack, and Y. Chen, (2008c), Estimating the physical top altitude of optically thick ice clouds from thermal infrared satellite observations using CALIPSO data, *Geophys. Res. Lett.*, *35*, L12801, doi:10.1029/2008GL033947.

Sherwood, S. C., J.-H. Chae, P. Minnis, and M. McGill (2004), Underestimation of deep convective cloud tops by thermal imagery, *Geophys. Res. Lett.*, *31*, 10.1029/2004GL019699.

Toon, O. B. and Co-authors (2009), Planning and implementation of the Tropical Composition, Cloud and Climate Coupling Experiment (TC4), *J. Geophys. Res.*, this issue.

Winker, D. M., W. H. Hunt, and M. J. McGill (2007), Initial performance assessment of CALIOP, *Geophys. Res. Lett.*, *34*, L19803, doi:10.1029/2007GL030135.

Xi, B., X. Dong, P. Minnis, and M. M. Khaiyer, 2009: A 10-year climatology of cloud cover and vertical distribution derived from both surface and GOES observations over the DOE ARM SGP site. Submitted to *J. Geophys. Res.*

Yang, P., G. W. Kattawar, G. Hong, P. Minnis, and Y. X. Hu (2008a), Uncertainties associated with the surface texture of ice particles in satellite-based retrieval of cirrus clouds: Part I. Single-scattering properties of ice crystals with surface roughness, *IEEE Trans. Geosci. Remote Sens.*, *46*(*7*), 1940-1947, doi:10.1109/TGRS.2008.916471.

Yang, P., G. W. Kattawar, G. Hong, P. Minnis, and Y. X. Hu (2008b), Uncertainties associated with the surface texture of ice particles in satellite-based retrieval of cirrus clouds: Part II. Effect of particle surface roughness on retrieved cloud optical thickness and effective particle size, *IEEE Trans. Geosci. Remote Sens.*, *46*(*7*), 1948-1957, doi:10.1109/TGRS.2008.916472.

Yang, S.-K., S. Zhou, and A. J. Miller (2006), *SMOBA: A 3-Dimensional Daily Ozone Analysis Using SBUV/2 and TOVS Measurements*. [Online]. Available: http://www.cpc.ncep.noaa.gov/products/stratosphere/SMOBA/smoba_doc.shtml

Yost, C. R., P. Minnis, J. K. Ayers, D. A. Spangenberg, A. J. Heymsfield, M. J. McGill, A. Bansemer (2009), Comparison of in situ and remotely sensed properties of deep convective clouds and anvils during TC4, *J. Geophys. Res.*, submitted for this issue.

Table Captions

Table 1. Cloud and radiation pixel-level parameters available for the post-experiment GOES-12 analyses.

Table 2. Coefficients for narrowband-to-broadband conversion formulae from July 2002 regression analyses.

Table 3. Mean domain cloud properties for the TC4 period from GOES-12.

Figure Captions

Figure. 1. GOES-10/12 visible-channel imagery for 24 July 2007 over the TC4 domain with ER-2 (blue) and DC-8 (red) flight track overlays. The inset graphs show the aircraft altitude as a function of UTC hour. (a) 1345 UTC, (b) 1445 UTC, (c) 1545 UTC, and (d) 1215 – 1845 UTC flight tracks on the 1528 UTC image.

Figure 2. Real-time cloud properties retrieved from GOES-12 data along the (a) ER-2 and (b) DC-8 flight tracks for 24 July 2007 illustrated in Figure 1. Note the differences in the scales for (a) and (b).

Figure 3. Pseudocolor images from satellite imagery taken at (a) 1545 UTC and (b) 1535 UTC, 24 July 2007. Note, in (a), GOES-10 data are used south of 10°N (northern Nicaragua).

Figure 4. Cloud ice crystal effective diameter D_e derived from 24 July 2007 GOES data at 1545 UTC and Terra MODIS data at 1535 UTC.

Figure 5. Mean cloud coverage for TC4 experiment (17 July – 8 August, 2007) from GOES-12.

Figure 6. Mean ice cloud coverage for TC4 experiment (17 July – 8 August, 2007) from GOES-12. (a) – (h) hours in UTC.

Figure 7. Mean cloud-top heights for TC4 experiment (17 July – 8 August 2007) from GOES-12.

Figure 8. Vertical distribution of cloud-top heights over greater TC4 domain, 17 July – 8 August 2007.

Figure 9. GOES-12 mean daytime cloud optical depth, 17 July – 8 August 2007. Domain coordinates the same as those in Figure 7.

Figure 10. Same as Figure 9, except for cloud effective particle size.

Figure 11. Same as Figure 9, except for cloud water path.

Figure 12. Mean daytime ice water path for TC4 experiment (17 July – 8 August, 2007) from GOES-12. Hours given in UTC.

Figure 13. Multi-layer and single-layer cloud retrievals for GOES-12, 2015 UTC, 5 August 2007.

Table 1. Cloud and radiation pixel-level parameters available for the post-experiment GOES-12 analyses.

Radiation & geometry	Standard Cloud Parameters	
0.65-µm reflectance	phase	effective emissivity, ε
10.8-µm temperature	optical depth, τ	liquid water path, LWP
3.9-10.8 µm BTD	particle size: r_e or D_e	ice water path, IWP
6.7-10.8 µm BTD	effective temperature, T_c	top height, Z_t
13.3-10.8 µm BTD	effective pressure, p_c	top pressure, p_t
SW albedo	effective height, Z_c	base height, Z_b
LW flux (OLR)	top temperature, T_t	base pressure, p_b
Latitude, longitude		
SZA,VZA, RAA		
COS and Multi-layer Cloud Parameters		
MCO2AT pressure, p_M	MCO2AT emissivity, ε_M	MCO2AT height, Z_M
multi-layer ID	upper-layer particle size, D_U	upper-layer pressure, p_U
upper-layer optical depth, τ_U	upper-layer temperature, T_U	upper-layer height, Z_U
upper-layer emissivity, ε_U	lower-layer particle size, r_L	lower-layer pressure, p_L
lower-layer optical depth, τ_L	lower-layer height, Z_L	lower-layer temperature, T_L

Table 2. Coefficients for narrowband-to-broadband conversion formulae from July 2002 regression analyses.

Fit	a_0	a_1	a_2	a_3	R^2	SE
SW albedo, ocean	0.01983	0.7628	-0.01485	0.0700	0.986	0.016
SW albedo, land	0.05646	0.6658	0.05843	0.0700	0.982	0.018
OLR	87.73	4.53	-0.00651	-0.159	0.974	6.3 Wm^{-2}

Table 3. Mean domain cloud properties for the TC4 period from GOES-12.

Parameter	Ice	Water
Cloud fraction, %	32.2	36.7
Cloud height	10.1	2.5
τ	6.9	7.6
Particle size, µm	46.5	15.3
Water path, gm^{-2}	123.9	67.6

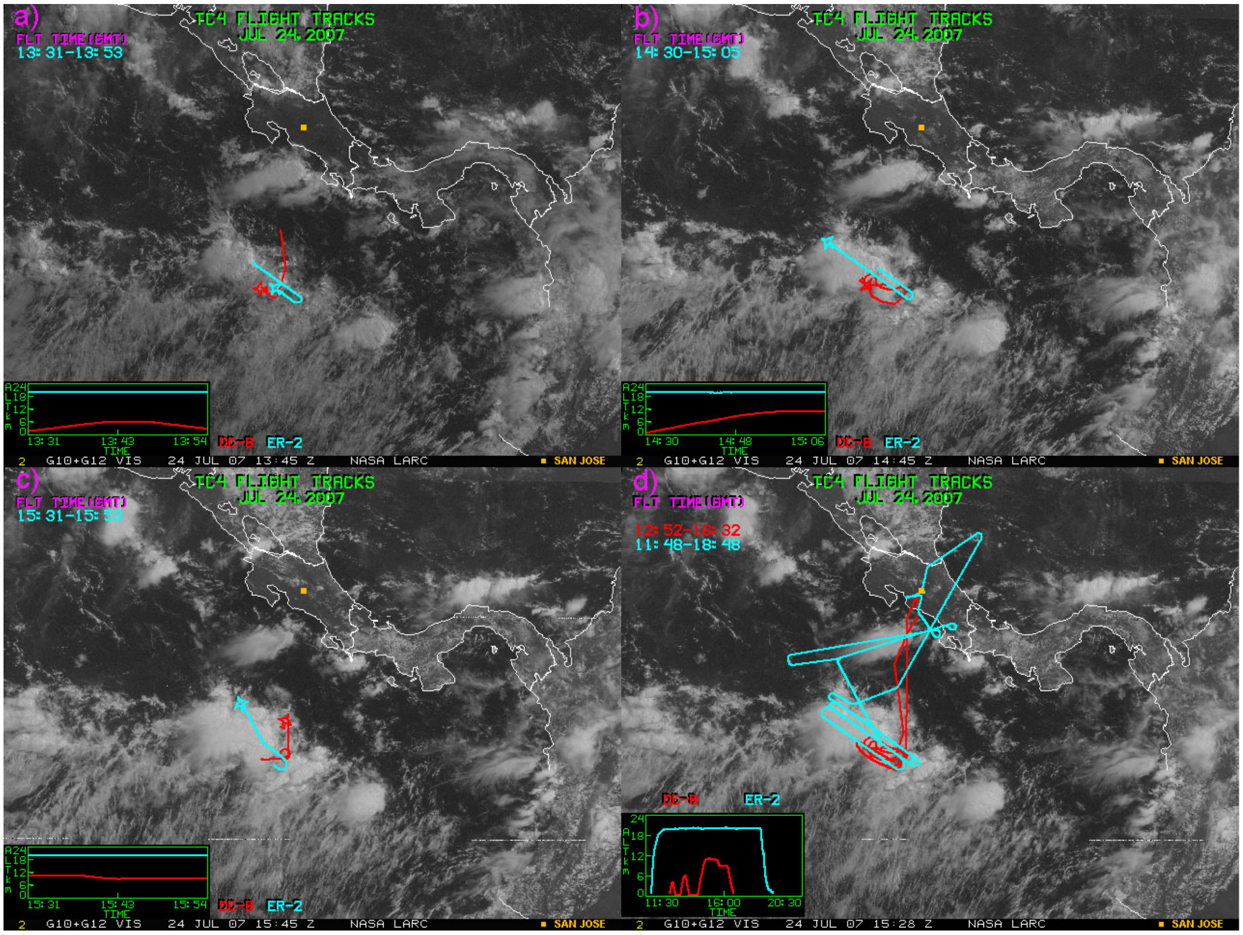

Figure. 1. GOES-10/12 visible-channel imagery for 24 July 2007 over the TC4 domain with ER-2 (blue) and DC-8 (red) flight track overlays. The inset graphs show the aircraft altitude as a function of UTC hour. (a) 1345 UTC, (b) 1445 UTC, (c) 1545 UTC, and (d) 1215 – 1845 UTC flight tracks on the 1528 UTC image.

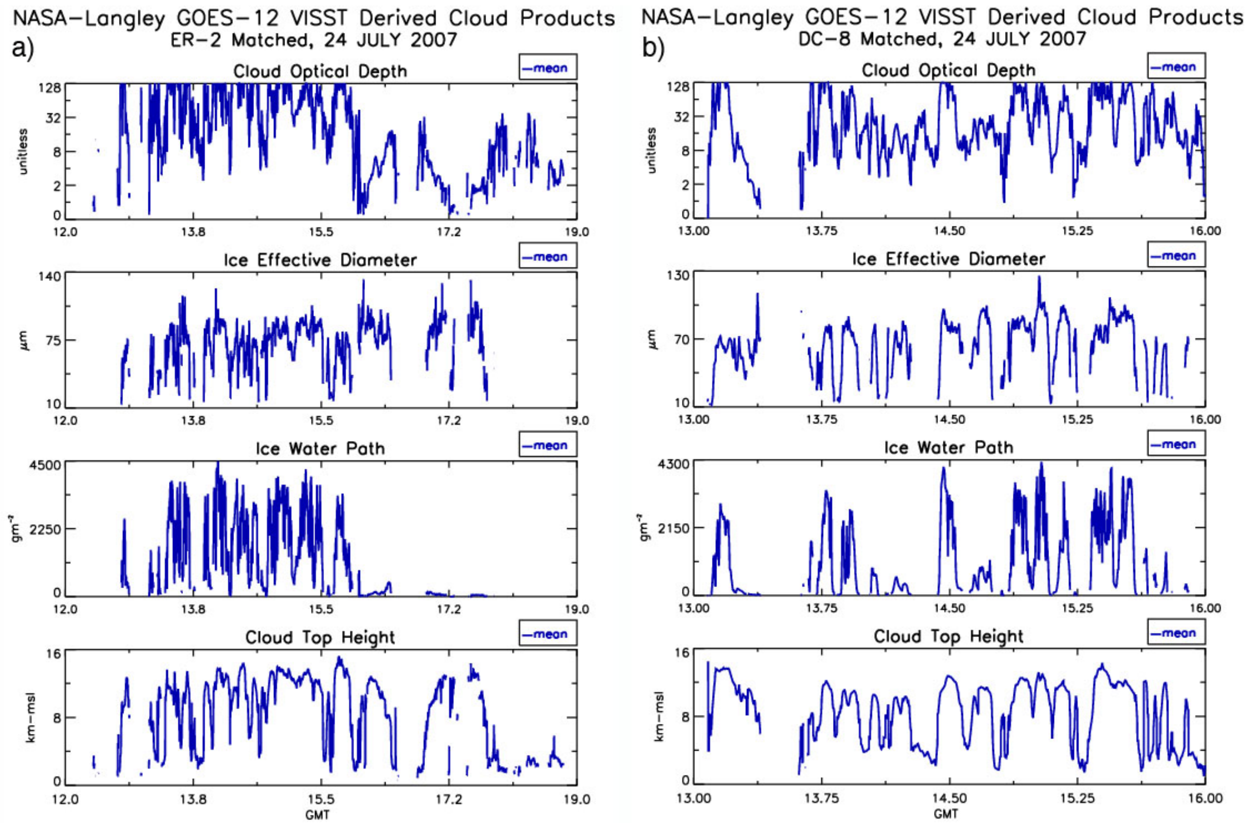

Figure 2. Real-time cloud properties retrieved from GOES-12 data along the (a) ER-2 and (b) DC-8 flight tracks for 24 July 2007 illustrated in Figure 1. Note the differences in the scales for (a) and (b).

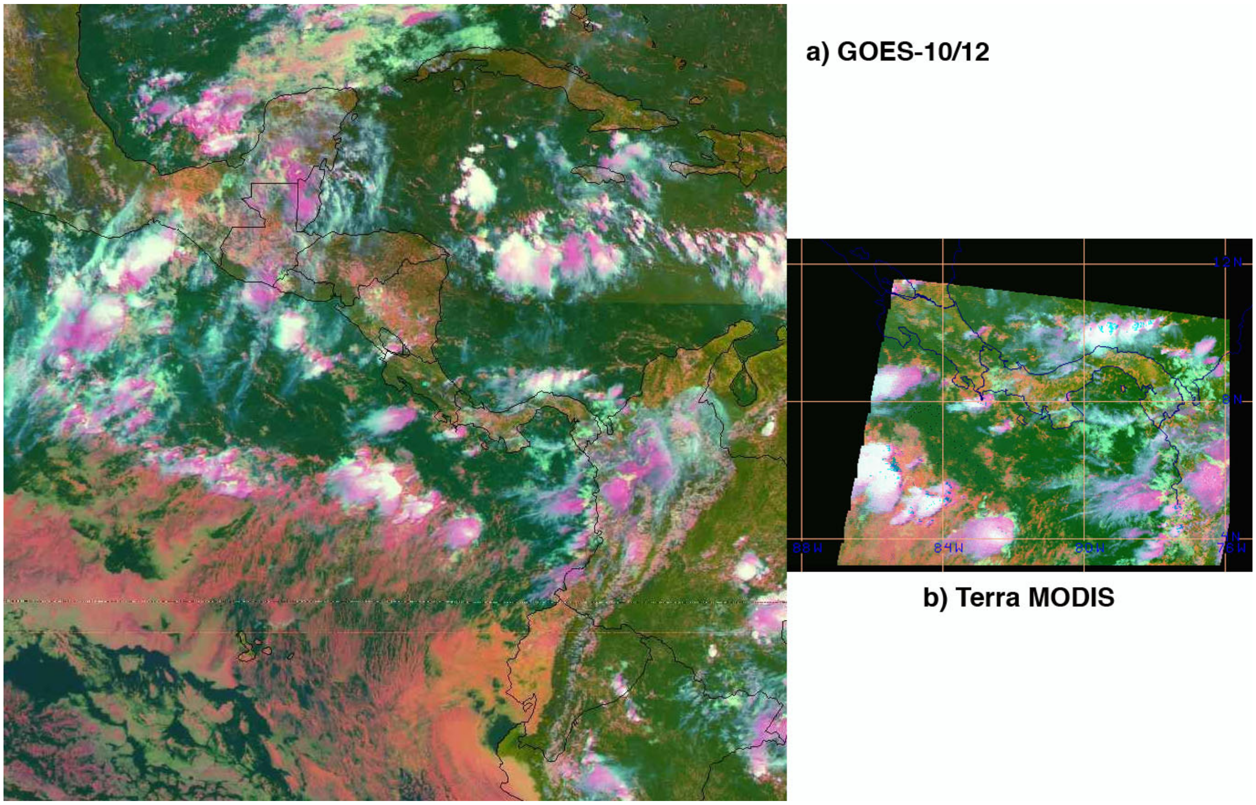

Figure 3. Pseudocolor images from satellite imagery taken at (a) 1545 UTC and (b) 1535 UTC, 24 July 2007. Note, in (a), GOES-10 data are used south of 10°N (northern Nicaragua).

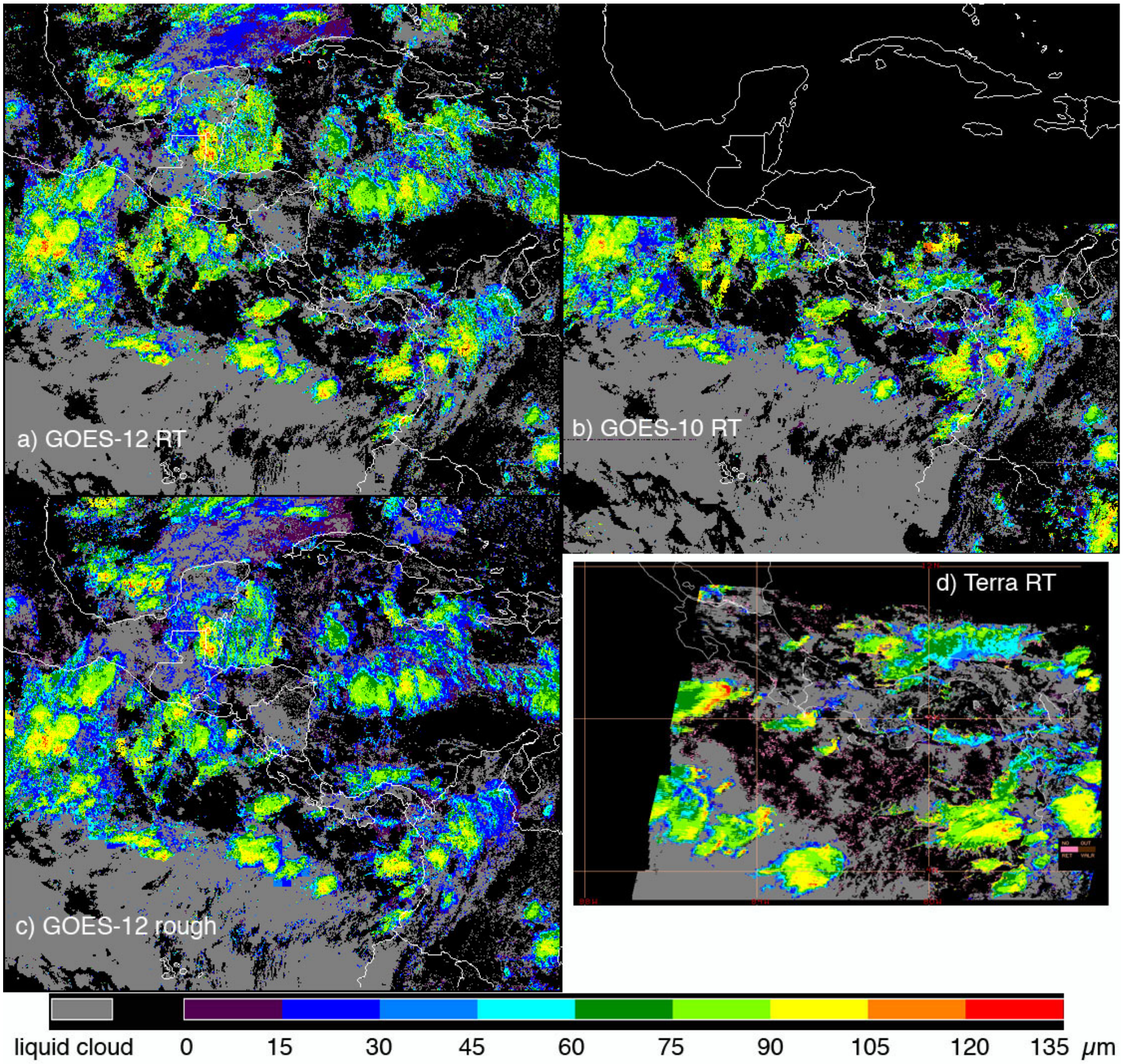

Figure 4. Cloud ice crystal effective diameter D_e derived from 24 July 2007 GOES data at 1545 UTC and Terra MODIS data at 1535 UTC.

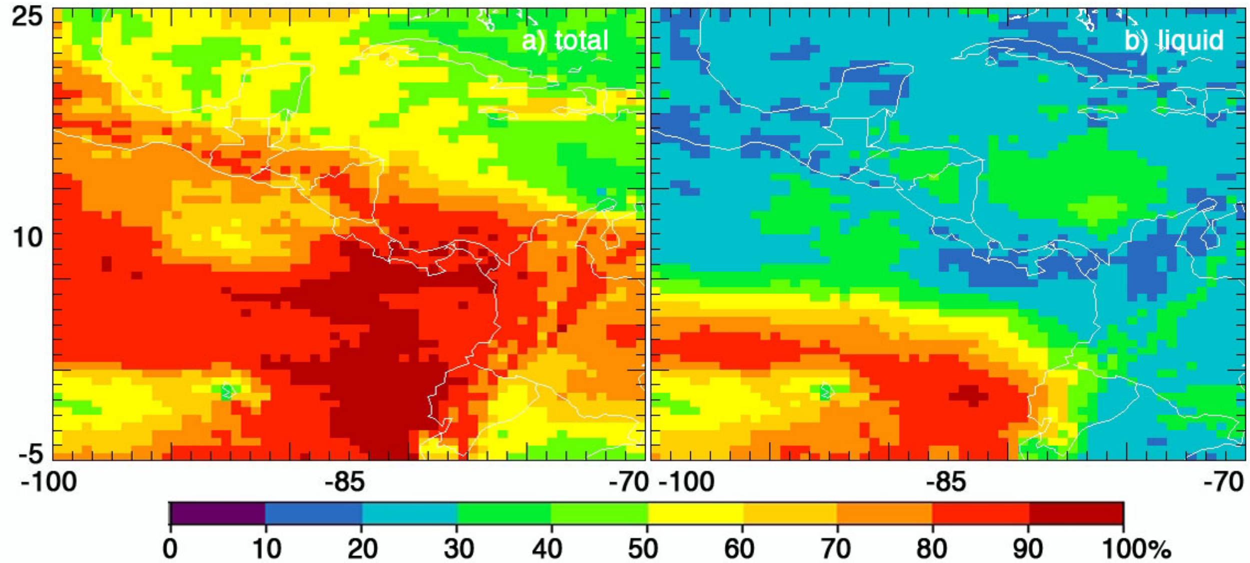

Figure 5. Mean cloud coverage for TC4 experiment (17 July – 8 August, 2007) from GOES-12.

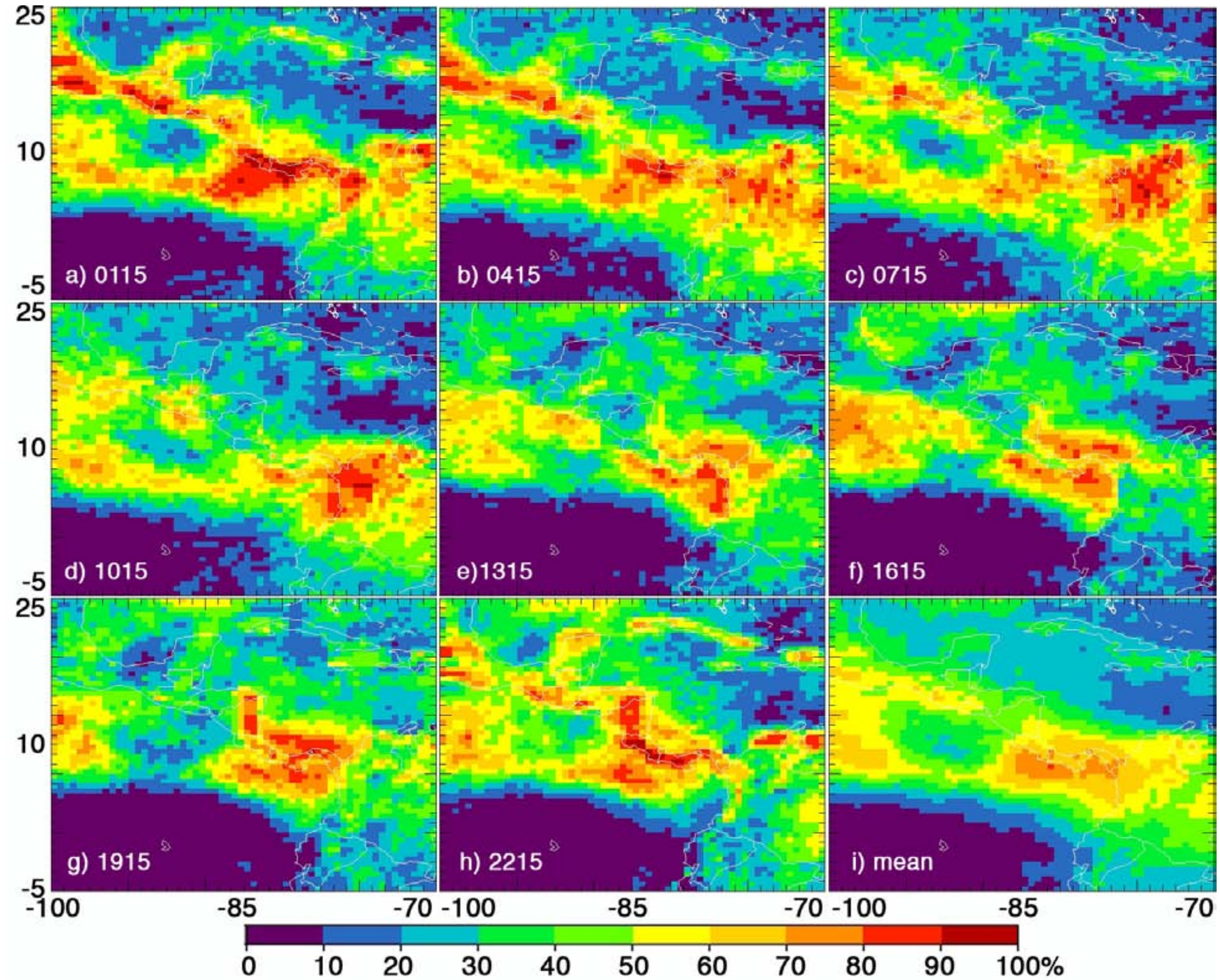

Figure 6. Mean ice cloud coverage for TC4 experiment (17 July – 8 August, 2007) from GOES-12. (a) – (h) hours in UTC.

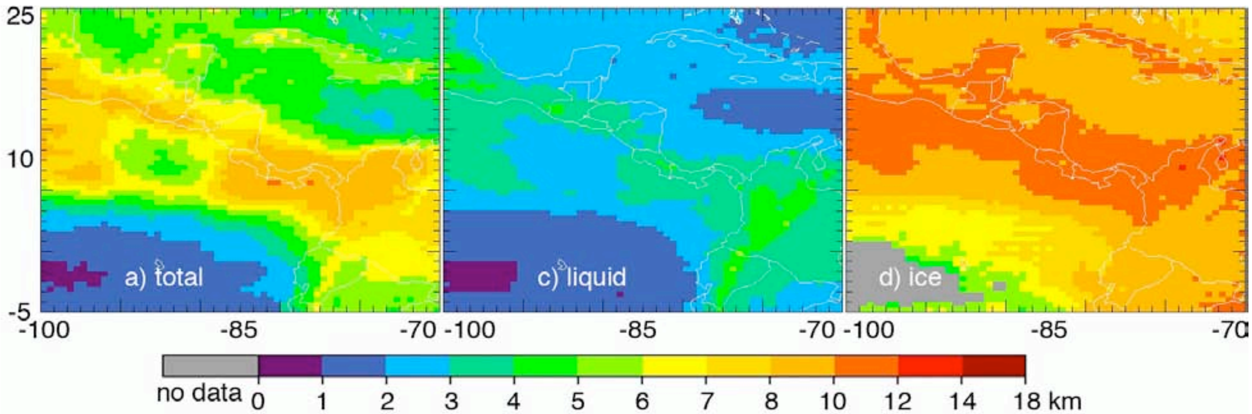

Figure 7. Mean cloud-top heights for TC4 experiment (17 July – 8 August 2007) from GOES-12.

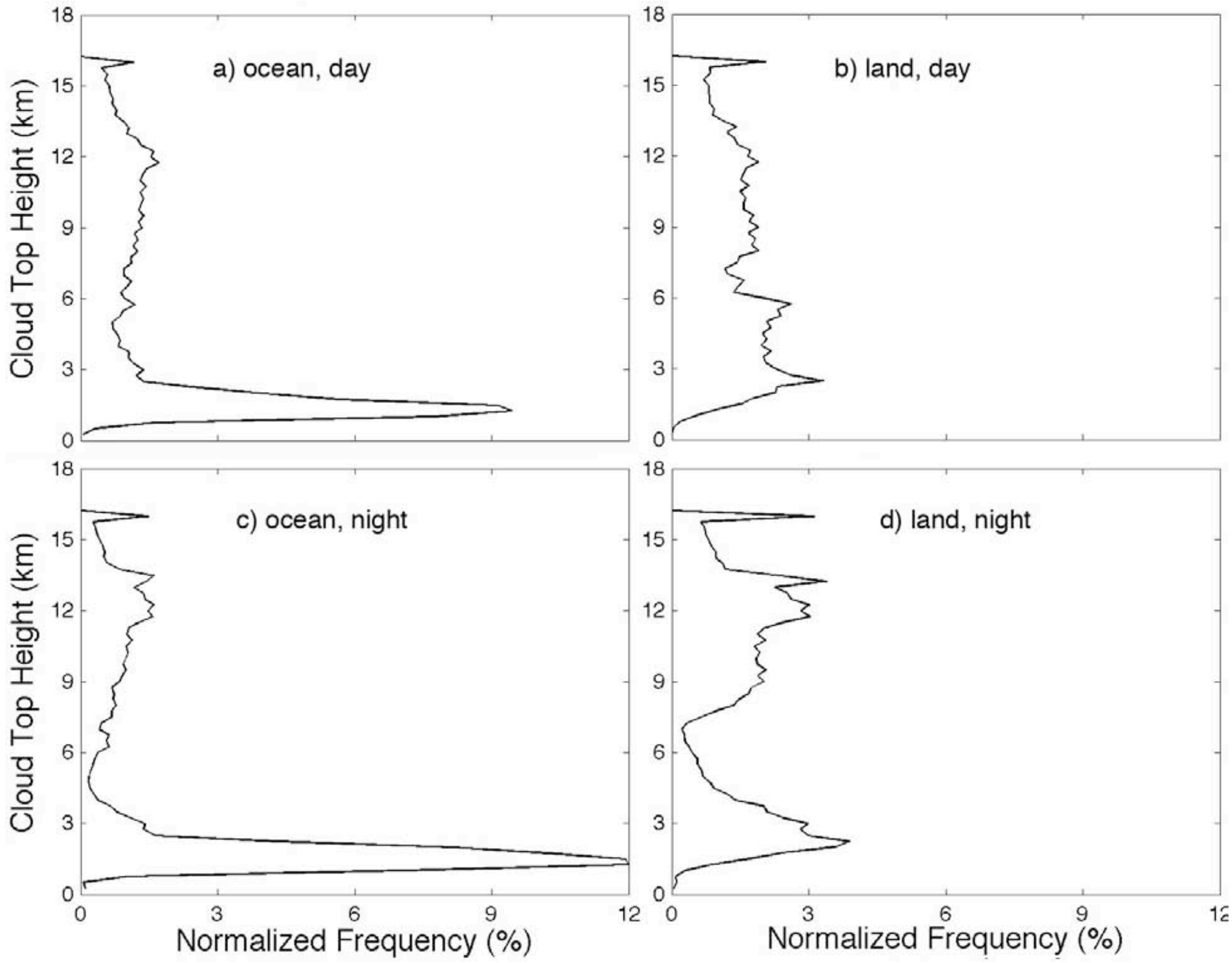

Figure 8. Vertical distribution of cloud-top heights over greater TC4 domain, 17 July – 8 August 2007.

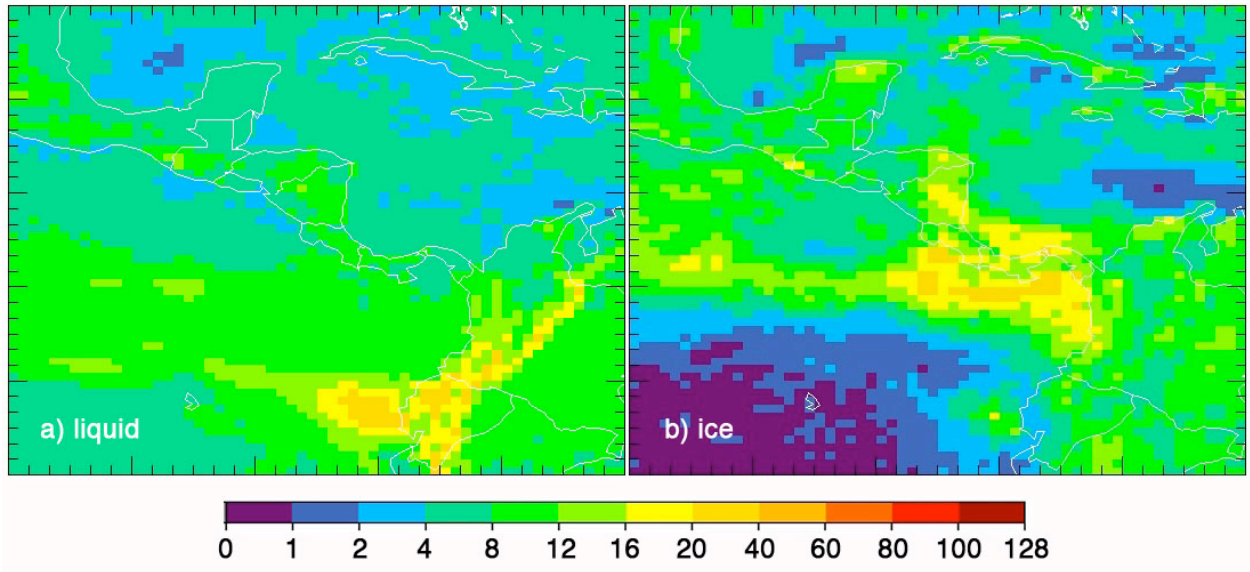

Figure 9. GOES-12 mean daytime cloud optical depth, 17 July – 8 August 2007. Domain coordinates the same as those in Figure 7.

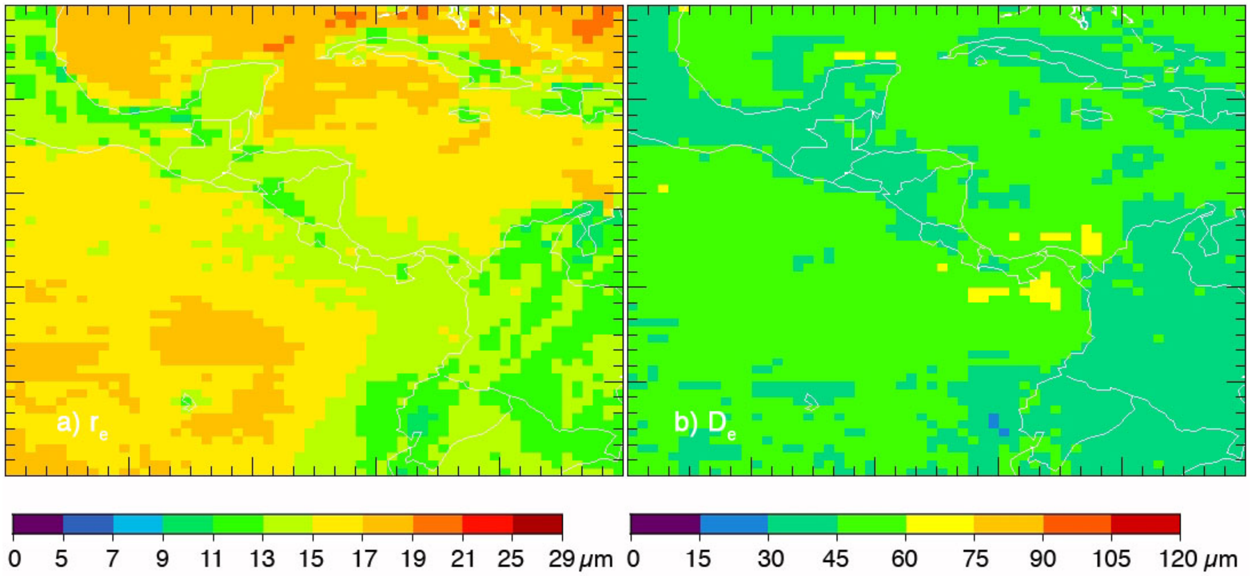

Figure 10. Same as Figure 9, except for cloud effective particle size.

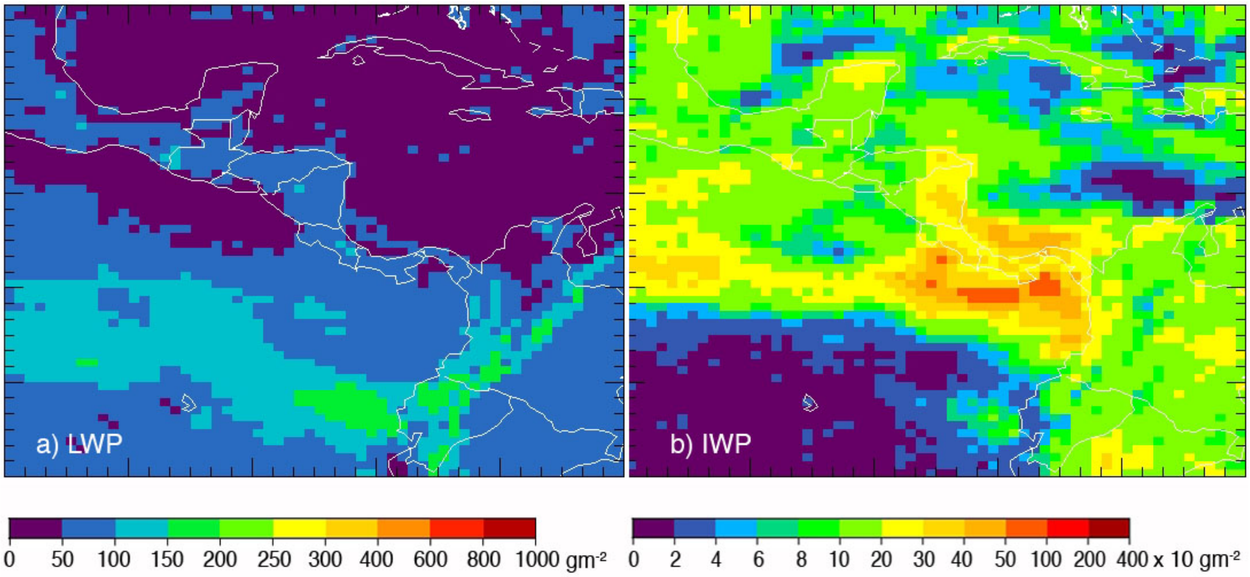

Figure 11. Same as Figure 9, except for cloud water path.

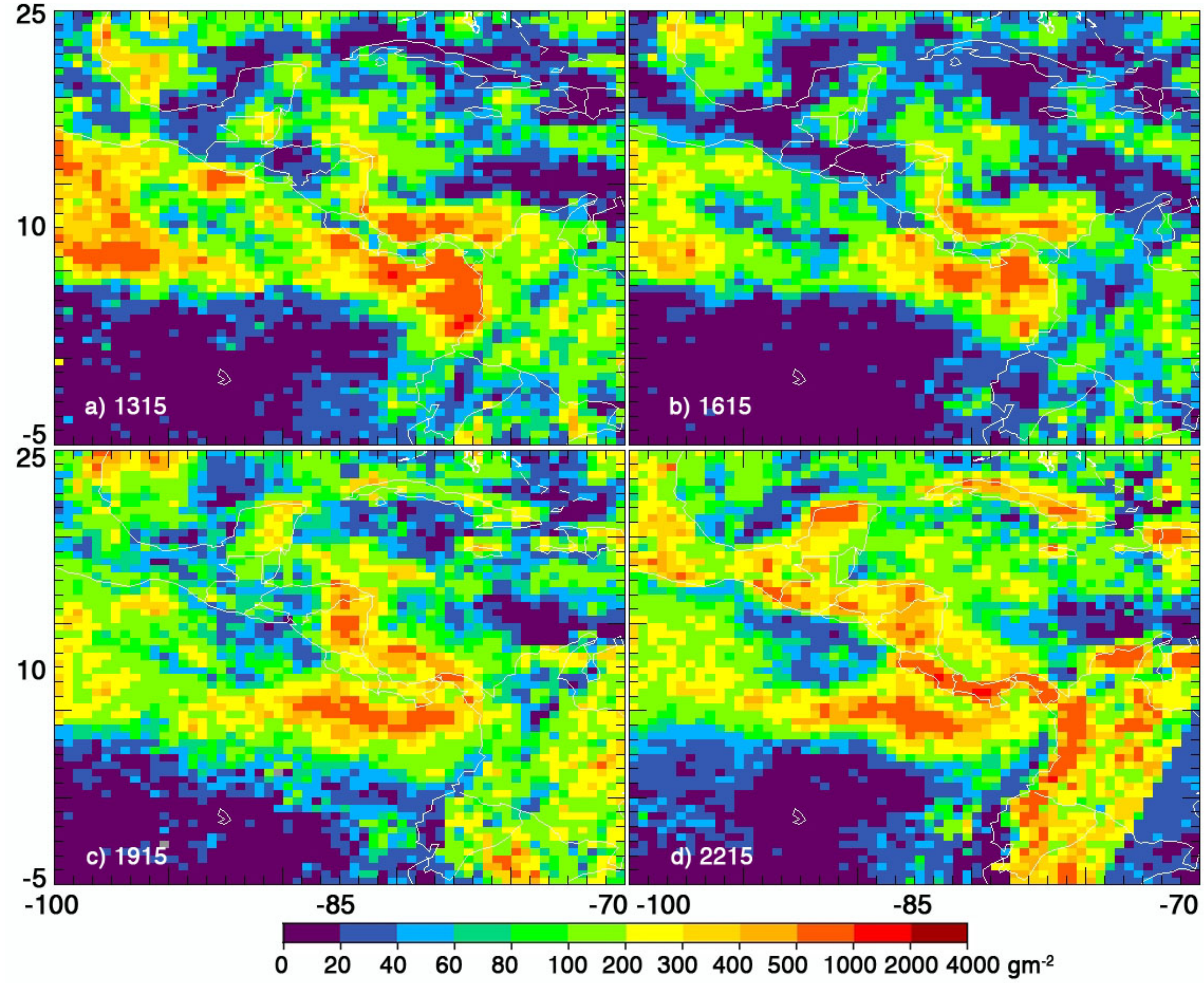

Figure 12. Mean daytime ice water path for TC4 experiment (17 July – 8 August, 2007) from GOES-12. Hours given in UTC.

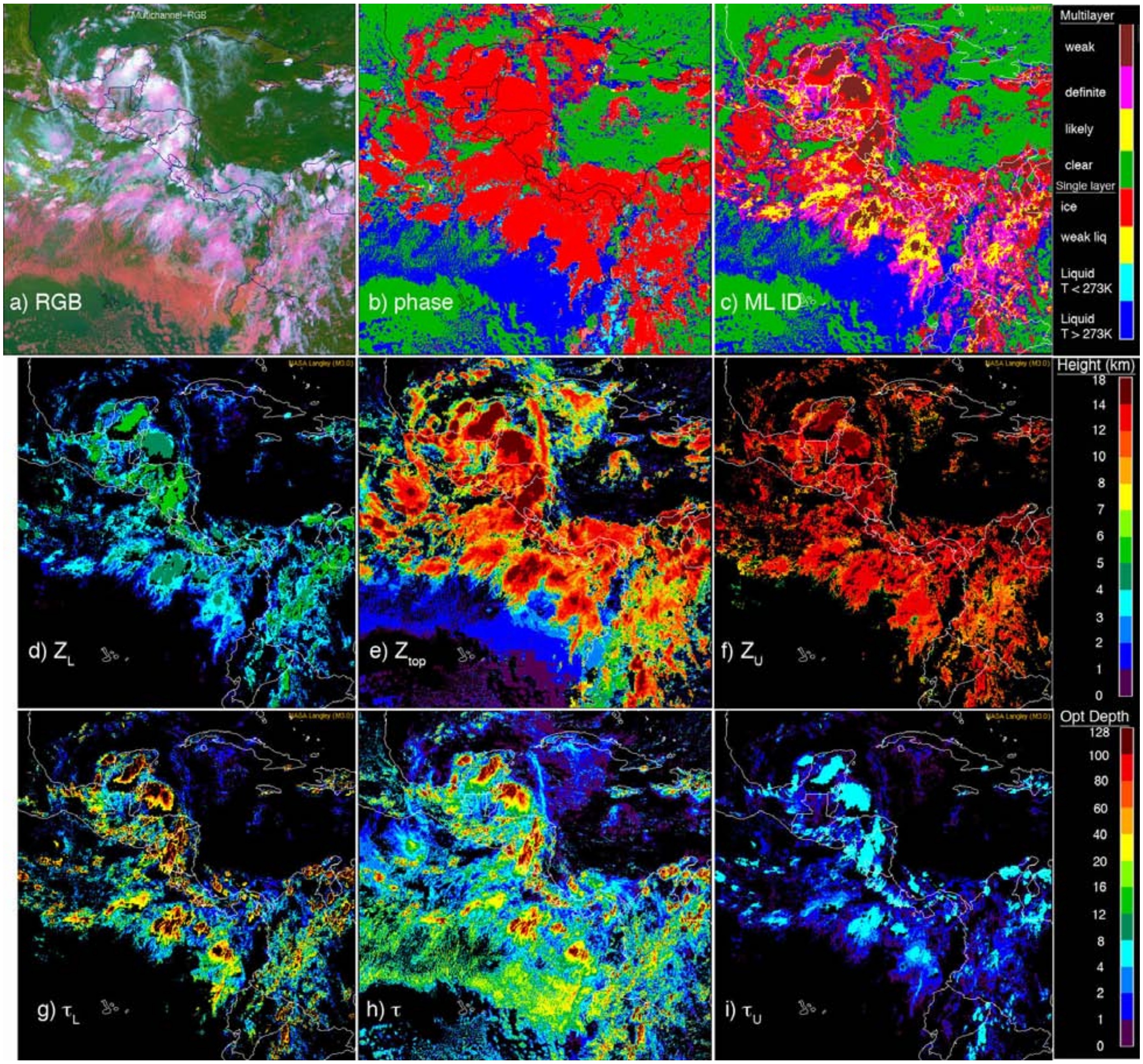

Figure 13. Multi-layer and single-layer cloud retrievals for GOES-12, 2015 UTC, 5 August 2007.